International Journal of Pressure Vessels and Piping 86 (2009) 541–549

Contents lists available at ScienceDirect

International Journal of Pressure Vessels and Piping

journal homepage: www.elsevier.com/locate/ijpvp

SCF analysis of a pressurized vessel–nozzle intersection with wall thinning damage

M. Qadir, D. Redekop*

Department of Mechanical Engineering, University of Ottawa, Ottawa, Canada K1N 6N5

ARTICLE INFO

Article history:
Received 15 May 2008
Received in revised form
8 October 2008
Accepted 22 January 2009

Keywords:
Finite elements
Tee joint
Stress concentration
Wall thinning

ABSTRACT

A three-dimensional finite element analysis is carried out of a pressurized vessel–nozzle intersection (tee joint), with wall thinning damage. A convergence-validation study is first carried out for undamaged intersections, in which comparisons are made with previously published work for the stress concentration factor (SCF), and good agreement is observed. A study is then carried out for specific tee joints to examine the effect on the SCF of varying the extent of the wall thinning damage. Finally, a parametric study is conducted in which the SCF is computed for a wide range of tee joints, initially considered undamaged, and then with wall thinning damage.

1. Introduction

The vessel–nozzle intersection (tee joint) is widely used in chemical plants, refineries and power plants (Fig. 1). Examples of tee joints include nozzles in heat exchangers, pressure vessels, or liquid storage tanks, and junctions in piping networks. Information about the behavior of this type of structure is important for developing design rules and safety criteria. Recently, interest has extended to tee joints damaged by wall thinning. With the rise in computer capability the analysis of such structures has now become feasible.

A series of recent papers have dealt with the wall thinning problem in the pressure vessels and piping field. Hwang et al. [1] have performed an experimental and numerical study seeking to identify the causes of shell wall thinning in a tee joint. There have been a number of studies on straight and curved pipes with wall thinning, including the works of Kim and Son [2], and Kim, Na, and Park [3]. Several studies have dealt with the effect of wall thinning on tee joints, including the works of Namita, Suzuki, and Abe [4], Takahashi et al. [5,6]. The issue of fatigue of tees with thinning is significant, but so far studies have only been for undamaged intersections [7–10].

There is vast literature on analytical solutions for the state of stress in pressurized tee joints (without wall thinning), extending from the work of Eringen and Suhubi [11] to Xue et al. [12]. These analytical solutions though apply only to thin shells. A number of finite element studies have dealt with this geometry, including the works of Moini and Mitchell [13], Dekker and Stikvoort [14], Finlayson et al. [15] and Diamantoudis and Kermanidis [16]. It has been established that three-dimensional elements are required to obtain accurate results for practical tee joints with a weld. Prior to the use of the finite element method many researchers [17–23] sought to develop simple equations to predict the SCF in tee joints. In the various investigations it was concluded that the diameter and thickness ratios, as well as the local characteristics at the junction, were primary factors affecting the SCF.

In this study a linear elastic finite element analysis (FEA) based on three-dimensional (3D) solid elements is performed to predict the SCF in pressurized tee joints (Fig. 1), without and with wall thinning damage. One aim of the study is to determine with maximum accuracy the SCF of tee joints using current FEA software. In a convergence-validation study it is shown that for undamaged tees the results obtained using the current method show good agreement with the experimental and other results given in the literature. The effect of the extent of the wall thinning damage on the SCF is assessed through the analysis of specific tee joints with varying extent of wall thinning. Then, a parametric study is conducted covering tee joints with a broad range of diameter and thickness ratios, and various depths of thinning. Finally, conclusions are drawn about the effect of wall thinning damage on the stress state of tees.

* Corresponding author. Tel.: +1 613 562 5800; fax: +1 613 562 5177.
E-mail address: dredekop@uottawa.ca (D. Redekop).

0308-0161/$ – see front matter © 2009 Elsevier Ltd. All rights reserved.
doi:10.1016/j.ijpvp.2009.01.010

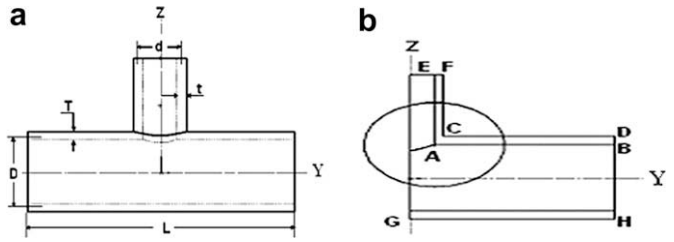

Fig. 1. Geometric details of a tee intersection, without wall thinning: (a) full geometry, (b) half-section through *YZ* plane.

2. Theoretical values for SCF for tees without wall thinning

The SCF is defined as the ratio of the maximum stress to the nominal stress. For internal pressure loading the nominal stress is given by $\sigma_n = PD/(2T)$, where P is the internal pressure, and T and D are respectively the thickness and mean diameter of the vessel (run pipe). The maximum stress is variously defined as the largest normal stress, the largest equivalent stress (von Mises stress, used for the current results), or the largest Tresca stress.

Prior to the availability of powerful numerical capabilities a number of simple formulas were developed for the SCF in pressurized tees, based on theoretical or experimental considerations. Subsequently, some simple formulas were developed based on statistical analysis of numerical results for tee joints determined using the FEA.

Lind [17], using the 'area method', developed the set of formulas

$$K_1 = \frac{\left[1 + 1.77(d/D)\sqrt{D/T} + (d/D)^2\sqrt{s/S}\right]\left[1 + (T/D)/\sqrt{s/S}\right]}{1 + (d/D)^2/(s/S)\sqrt{s/S}}$$

$$K_2 = \frac{\left[1.67\sqrt{s/S}\sqrt{D/T} + 0.565(d/D)\right]\left[1 + (T/D)/\sqrt{s/S}\right]}{0.67\sqrt{s/S}\sqrt{D/T} + 0.565(d/D)/(s/S)}$$

$$\mathrm{SCF} = \max\{K_1, K_2\} \tag{1}$$

where $s = d/(2t)$, $S = D/(2T)$, and t, d are the thickness and the mean diameter of the nozzle.

Expressions for the SCF were given by Money [18], on the basis of experimental results for many tee joints. According to his work, SCF formulas valid for $r/R < 0.7$ and $r/R > 0.7$, respectively, are given by

$$\mathrm{SCF} = 2.5\left[\left(\frac{r}{t}\right)^2\frac{T}{R}\right]^{0.2042} \quad \text{and} \quad \mathrm{SCF} = 2.5\left[\left(\frac{r}{t}\right)^2\frac{T}{R}\right]^{0.24145} \tag{2}$$

In these two relations R and r are the mean radii of the vessel and nozzle. Clearly, there is discontinuity at $r/R = 0.7$, which arises from the author's representation of the available results by two separate branch curves.

Decock [19], based on results from experimental data, presented a formula for the SCF in terms of non-dimensional parameters as:

$$\mathrm{SCF} = \frac{\left[2 + 2\frac{d}{D}\sqrt{\left(\frac{d}{D}\times\frac{t}{T}\right)} + 1.25\frac{d}{D}\sqrt{\frac{D}{T}}\right]}{\left[1 + \frac{t}{T}\sqrt{\left(\frac{d}{D}\times\frac{t}{T}\right)}\right]} \tag{3}$$

This correlation equation was considered applicable to the determination of the SCF at the crotch corner of a tee joint.

More recently Gurumurthy et al. [20], based on a shell theory FEA parametric study, developed a formula for the SCF as

$$\mathrm{SCF} = 1.75(T/t)^{0.4}(d/D)^{-0.08}(\lambda)^{0.6} \tag{4}$$

where $\lambda = d/(DT)^{1/2}$ is the pipe factor.

Moffat et al. [21,22] have derived a formula for the effective stress factor (ESF) based on a parametric analysis of tees using three-dimensional FEA. The ESF is essentially equivalent to the SCF. The formula for the ESF is given by

$$\begin{aligned}\mathrm{ESF} = {} & \left[a_1 + a_2(d/D) + a_3(d/D)^2 + a_4(d/D)^3\right] + \left[a_5 + a_6(d/D)\right. \\ & \left. + a_7(d/D)^2 + a_8(d/D)^3\right](t/T) + \left[a_9 + a_{10}(d/D)\right. \\ & \left. + a_{11}(d/D)^2 + a_{12}(d/D)^3\right](D/T)^p + \left[a_{13} + a_{14}(d/D)\right. \\ & \left. + a_{15}(d/D)^2 + a_{16}(d/D)^3\right](t/T)(d/T)^p\end{aligned} \tag{5}$$

where $p = 1.2$, and the constants a_1–a_{16} are given by 2.5, 2.715, 8.125, −6.877, −0.5, −1.193, −5.416, 5.2, 0.0, 0.078, −0.195, 0.11, 0.0, −0.043, 0.152, −0.097.

3. Finite element modeling

The commercial package ADINA 8.3.3 [24] was used for the current numerical analysis. The elements available for three-

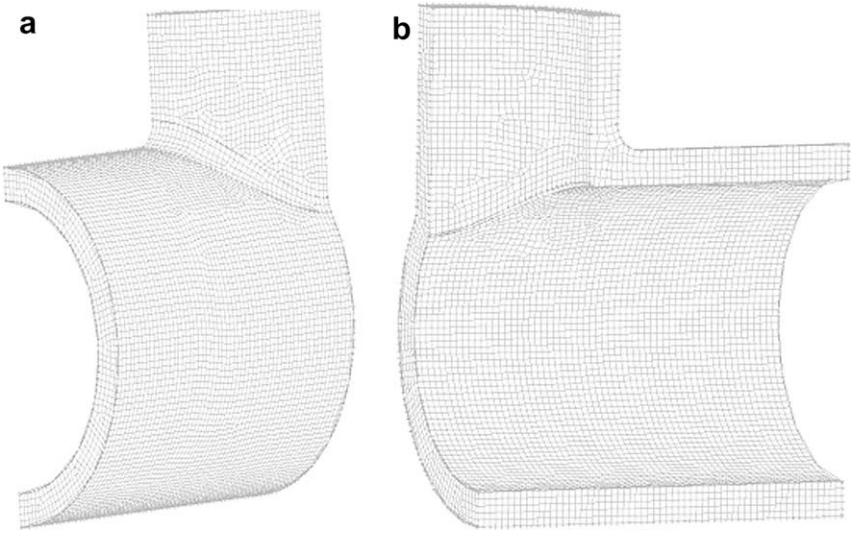

Fig. 2. View of the details of the model: (a) outside view showing the fillet weld at the outer junction, (b) inside view showing slight rounding at the inner junction.

Table 1
Geometric description and partial results for the validation-convergence models.

Model	Table, model in Ref. [21]	Geometric parameters			Type	SCF		
		d/D	t/T	D/T		Ref. [21]	FEA	Diff. %
V1	T5, M1	0.09	1.13	36.1	FEA	2.55	2.339	−8.3
V2 (C1)	T5, M4	0.20	0.20	8.0	Expt.	3.25	3.242	−0.2
V3	T4, M7	0.25	0.57	16.5	Expt.	3.40	3.215	−5.4
V4	T4, M2	0.31	0.40	17.9	Expt.	3.40	3.853	13.3
V5 (C2)	T5, M12	0.50	0.50	11.0	FEA	4.23	4.304	1.7
V6	T4, M14	0.55	0.91	57.6	Expt.	4.90	5.775	17.9
V7	T5, M14	0.62	1.00	15.1	Expt.	3.70	4.225	14.2
V8	T5, M13	0.62	0.62	10.0	FEA	4.24	4.783	12.8
V9	T4, Craw.	0.66	0.64	18.9	Expt.	4.53	4.376	−3.4
V10	T4, M3	0.69	0.63	156.0	FEA	4.08	4.789	17.4
V11	T4, M5	0.76	1.50	10.3	Expt.	3.50	3.186	−9.0
V12 (C3)	T4, M10	1.00	1.00	19.0	Expt.	5.40	6.013	11.4

dimensional analysis in this software include both hexahedral (brick) and tetrahedral ones, and both types were considered in the convergence-validation part of this study. The analysis was for a quarter tee model, accounting for the symmetry that exists in a pressurized tee about the longitudinal *YZ* plane, and the transverse *XZ* plane (Fig. 1). The nodes on the planes of symmetry were constrained against motion in the direction perpendicular to the plane, as well as against out-of-plane rotations. The end of the vessel was subject to an axial pressure loading corresponding to closed end conditions. A similar pressure loading was applied in the axial direction on the nozzle.

Fillet welded joints such as tee, lap and corner joints are the most common connection in welded fabrication. Details of the current FEA modeling of tees, showing an outer fillet radius and an inner rounding at the junction, are shown in Fig. 2. A circular curve has been inserted at the junction of the outer surfaces of the two components (position C of Fig. 1b), representing a fillet weld. The size of the fillet was adjusted for each model to a value that would closely approximate the weld size used in industry. No attempt has been made to incorporate notches or cracks into the model. A small rounding (about 2–3 mm radius) at the inner surfaces of the intersection (position A of Fig. 1b) is provided to eliminate the sharp corner at the inside of the junction. While stress concentration is highly dependent on the local geometry, the current results, provided in later sections of the paper, show remarkable agreement with previous work, for which geometric details may have been defined somewhat differently.

A linear elastic analysis was conducted throughout this study. The material properties used were: Young's modulus = 210,000 MPa, Poisson's ratio = 0.3.

4. Convergence study

A convergence study was carried out in order to describe the variation in FEA results due to mesh refinement. Three convergence models, C1, C2, and C3 were considered, covering tees of various diameter and thickness ratios. Geometric details of the models are included in Table 1. Some sample meshes from the convergence study for model C2 are given in Fig. 3.

Results were obtained for selected mesh densities for the three models as shown in Table 2. For model C1, meshes consisting of both 10-node tetrahedral and 8-node brick elements were used. With mesh refinement, convergence of the SCF is clearly observed for the series of models of both types of elements. The numerical stability in the analysis of models with tetrahedral elements was in general less than with brick elements. For models C2 and C3, meshes consisting only of 8-node brick elements were used. For both of these models, convergence is clearly observed as the mesh is refined. A set of results using 27-node brick elements was also obtained, showing a difference of less than 0.05% relative to the results using 8-node brick elements. The increase in computational time and file size though was by a factor as large as 10. In consideration of these results, meshes consisting of 8-node brick elements, having a density of about four elements over the run pipe thickness, were selected for further work in the study.

5. Validation study

Twelve models (V1–V12), as described in Table 1, were studied to validate the current FEA process for determining the SCF. Each of these models has been featured in a previous FEA or experimental study (a summary is given by Moffat et al. [21]). For these models the ranges in the geometric parameters are as follows – d/D: 0.09–1.00, t/T: 0.2–1.5, and D/T: 8.0–156. A comparison is given in Table 1 of the SCF results from previous studies cited in Ref. [21] (indicated by the abbreviation 'Ref.'), and the current study ('FEA'). The range in the differences of the current values from the previous ones is from −9.0% to +17.9%, with an average difference of +5.2%. A positive average difference was expected, in view of the better capability of the 3D FEA to capture local stress peaks. In evaluating the results, it should be noted that there were inevitably slight geometric differences in the models of the past and current studies.

In Table 3 a comparison is given of the SCF results obtained by the approximate formulas of Eqs. (1–5) and the current FEA approach. The previous experimental-numerical ('Ref.') values are repeated for convenience. For each of the approximate formulas and for the FEA, the minimum, maximum, and average differences relative to the reference values are stated. It is noted that the

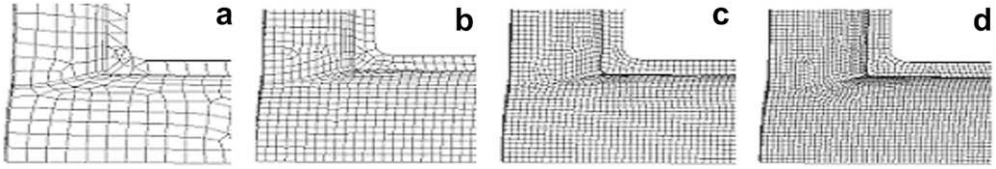

Fig. 3. (a–d) Partial mesh plots for convergence model C2 showing 1–4 elements over the thickness.

Table 2
Comparison of results for the SCF in the convergence study.

Model	Element type	Nodes per element	Elements per unit length	Max. element size (mm)	Total elements (k)	SCF
C1 (V2)	Tetra	10	1	19.0	3.0	3.286
			2	9.5	14.4	3.717
			3	6.33	69.8	3.364
			4	4.75	94.9	3.484
	Brick	8	1	19.0	2.3	2.621
			2	9.5	6.2	2.973
			3	6.33	15.0	3.092
			4	4.75	29.9	3.215
			5	3.8	53.1	3.227
C2 (V5)	Brick	8	1	21.0	2.4	3.862
			2	10.5	7.7	4.162
			3	7.0	17.3	4.217
			4[a]	5.25	33.9	4.225
C3 (V12)	Brick	8	1	4.2	6.5	1.932
			2	2.1	31.9	2.108
			3	1.4	42.6	2.316
			4	1.05	107.3	2.339

[a] Mesh type and size used in the parametric study.

formula values relative to the reference value are significantly higher for model V7, and significantly lower for model V12. The current FEA values agree much more closely with the reference values than do the formula values.

As discussed in Section 2, the theoretical formulas (Eqs. 1–5) can give quick predictions of the SCF values. In developing these formulas each corresponding author used a limited range for the geometric parameters (t/T, d/D, D/T), over which good predictive results may be expected. The FEA is more independent of the range of geometric parameters, and can give dependable results provided there is correct usage of element type and mesh density, and accurate modeling of the domain, material, loading, and boundary conditions. For the present validation models, the Money [18] and Moffat [21] correlation equations, Eqs. (2) and (5) respectively, gave the most satisfactory results. The formulas given by Lind [17] and Decock [19] generally gave conservative results. The Gurumurthy formula [20] gave results which were significantly conservative on the average, and which also showed a greater fluctuation than the other formulas.

In a further evaluation of the current approach, special attention is given to a comparison of the current results with the results for the experimental models of Table 1 (taken from Ref. [21]). In Fig. 4, plots of the SCF versus the diameter ratio are presented for these models. Generally there is good agreement between the two sets of results. Some differences though arise in the range $d/D = 0.3$ to $d/D = 0.6$, and these may partially be explained by limitations in the experimental procedures. Finite-length strain gauges used in

Table 3
SCF – comparison of reference and FEA values with formula values for the validation study.

Model	Lind	Money	Decock	Gurum.	Moffat	Ref.	FEA
V1	2.710	3.325	2.680	2.154	3.228	2.55	2.339
V2	2.587	2.725	2.846	2.462	3.193	3.25	3.242
V3	3.195	3.519	3.381	3.622	3.681	3.40	3.215
V4	5.446	4.029	4.864	7.913	4.568	3.40	3.853
V5	3.485	3.101	3.349	4.359	3.800	4.23	4.304
V6	4.894	4.094	4.549	6.397	4.631	4.90	5.775
V7	10.156	3.653	9.667	7.764	6.288	3.70	4.225
V8	2.715	2.657	2.565	3.663	3.085	4.24	4.783
V9	5.113	3.963	4.724	7.646	4.725	4.53	4.376
V10	3.657	3.548	3.658	4.045	4.239	4.08	4.789
V11	3.855	3.684	3.769	4.308	4.455	3.50	3.186
V12	1.778	1.478	2.009	1.096	2.255	5.40	6.013
Min %	−67.1	−72.6	−62.8	−79.7	−58.2	–	−9.0
Max %	174.5	30.4	161.3	132.7	69.9	–	17.9
Ave %	8.8	−11.5	5.6	20.1	6.0	–	5.2

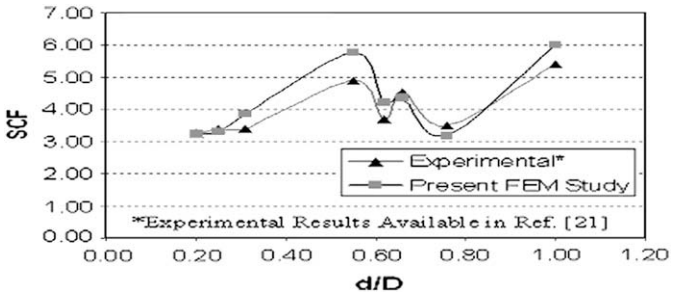

Fig. 4. Validation study – comparison of experimental results for the SCF with the present FEA results.

experimental studies cannot exactly represent peak stresses in areas of high stress gradient. A reported maximum stress value may then be lower than that which actually occurs in the physical model. Using elements that are finite, the FEA also has this difficulty, but the difficulty can be controlled by refining the mesh, and using higher order elements. Overall, it is considered that the current 3D FEA gives reliable predictions for the SCF over the full range of geometries studied.

6. Parametric models

The American National Standards Institute (ANSI) assigns 'schedule numbers' to classify wall thickness for different pressures. ANSI covers all pipe sizes from NPS 1/8″ through NPS 48″ (3.175–1219.2 mm), and all wall thicknesses through ANSI 36.19-B36.10 [25]. Grouping is according to three main schedules, identified as standard (STD), extra strong (XS) and double extra strong (XXS). For the parametric models of this study, a 10 inch (254 mm) nominal pipe size (NPS) is selected for the vessel or run pipe. For the nozzle, sizes varying from NPS ½″, 1″, 3″, 6″, to 8″ (12.7–203.2 mm) are selected, to represent a range in the d/D ratio.

A total of 20 models were selected for the parametric study, with geometric properties as given in Table 4. In this table d and D represent the mean nozzle and pipe diameters. The models are grouped together in four categories, based on the run pipe (vessel) schedule. Models 1–5 are according to schedule XXS, models 6–10 according to schedule XS, models 11–16 according to schedule S40S (STD), and models 16–20 according to schedule S10S (relatively thinnest). The ranges in the geometric parameters are as follows; nozzle–vessel diameter ratio: $0.05 \le d/D \le 0.8$, nozzle–vessel

Table 4
Geometric description of the parametric models.

Model	D (mm)	T (mm)	d (mm)	t (mm)	d/D	t/T	D/T	SCF
1	247.6	25.4	13.93	7.41	0.05	0.29	10.75	2.44
2			24.31	9.09	0.1	0.36		2.47
3			73.66	15.24	0.3	0.6		2.98
4			146.3	21.94	0.6	0.86		3.67
5			196.9	22.23	0.8	0.88		4.21
6	260.3	12.7	17.6	3.73	0.05	0.29	21.5	2.31
7			28.85	4.55	0.1	0.36		2.51
8			81.28	7.62	0.3	0.6		3.13
9			157.3	10.97	0.6	0.86		3.90
10			206.4	12.7	0.8	1		4.86
11	263.73	9.27	18.58	2.76	0.05	0.3	29.45	2.33
12			30.02	3.38	0.1	0.36		2.51
13			83.41	5.49	0.3	0.59		3.45
14			161.2	7.11	0.6	0.77		4.56
15			210.9	8.18	0.8	0.88		6.92
16	268.81	4.19	19.23	2.11	0.05	0.5	65.14	2.46
17			30.63	2.77	0.1	0.66		2.59
18			85.85	3.05	0.3	0.73		4.18
19			164.9	3.4	0.6	0.81		7.08
20			215.3	3.76	0.8	0.9		9.57

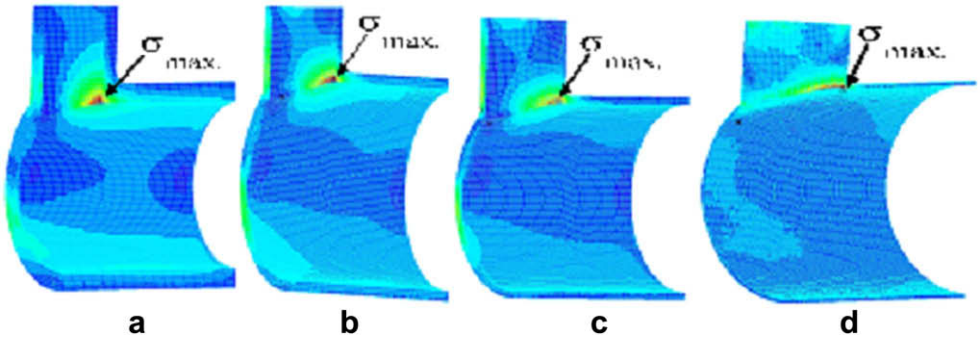

Fig. 5. Contours of von Mises stress in undamaged tees having the same diameter ratio, $d/D = 0.6$, but different schedules: (a) model 4 (schedule XXS), (b) model 9 (schedule XS), (c) model 14 (schedule STD), (d) model 19 (schedule S10S).

thickness ratio: $0.29 \le t/T \le 0.9$, and vessel diameter-thickness ratio: $10.75 \le D/T \le 65.14$.

A study of the parametric tees in undamaged conditions was first carried out. Values for the calculated SCF are given in the final column of Table 4. Fig. 5 describes the spatial change in the von Mises stress level arising in a set of tees having solely a change in thickness of the run pipe and nozzle. In viewing Fig. 5a–d in an increasing sequence, the effect on the von Mises stress of decreasing the thickness is observed. The high stress zone in the junction area consistently increases as the thickness decreases, with the highest stress occurring at the crotch corner in all four cases. In the axial directions of both the vessel and nozzle the region of high stress intensity steadily widens as the model thickness decreases.

To define the main geometry of a tee joint, three main parameters are required; t/T, d/D and D/T. Calculated SCF values are given in the last column of Table 4 for each of the models of the four groups considered. Plots of the SCF versus the d/D ratio of the undamaged parametric models for different D/T ratios are shown in Fig. 6 for each of the four main groups. The t/T ratio for each model is proportional to the d/D ratio as per the dimensions given in the ANSI standard. Relations between the SCF values with the geometric ratios can be used to find the dimensions of both components (vessel and nozzle) corresponding to a certain admissible value of the SCF in the design of the tee joint. Conversely, the SCF values can be estimated for an existing tee geometry.

7. Modeling of wall thinning

Detailed information of actual wall thinning in existing tees is difficult to obtain for the many possible industrial situations. In the modeling of wall thinning for theoretical analysis, several factors must be taken into account. From past studies of tees with wall thinning [1,4,5], it is clear that several positions in the vicinity of the intersection are potentially at risk. In Ref. [1], the damage in tees of nuclear power plants was indicated as having occurred around the impingement baffles. In Ref. [4], it is indicated that the forms of the thinned-wall portions were determined by the flow pattern of the internal water at tees, but details were not provided. In Ref. [5], the damage in a tee was modeled as occurring at the intersection of the center line of the nozzle with the opposite wall of the run pipe. In Ref. [6] the damage in a pipe with a transverse orifice was assumed to have occurred at a short axial distance away from the center of the orifice. Generally, in these studies inner-wall non-uniform thinning was assumed.

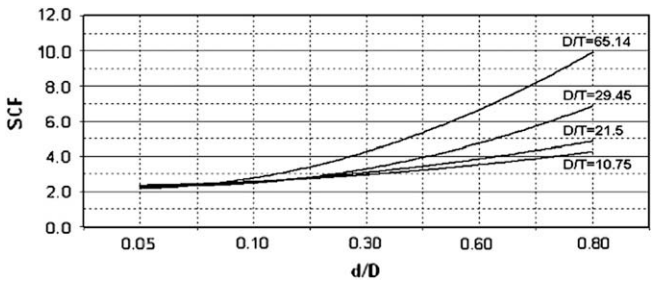

Fig. 6. Plots of the SCF in undamaged tees with the d/D ratio for different D/T ratios (results apply to tees with nozzle thickness and fillet welds as discussed in Section 6).

For the present study, the modeling of thinning was chosen considering past modeling of thinning, expected thinning pattern due to erosion/corrosion, severity of the effect of thinning, and computational limitations. Several patterns were examined before a final configuration was selected for detailed study. In consideration that the wall thinning was mainly due to localized erosion/corrosion surrounding the junction, and that the highest stress in undamaged tees occurs at the crotch corner, the maximum thinning in this study was modeled at the inner wall at the junction. In erosion/corrosion situations it is reasonable to expect that the extent (mid-surface distance) of thinning away from the junction for a small nozzle is less than for a large nozzle. As well, one can expect that the depth of thinning decreases with the distance away from the junction. Thus in this study, the extent of the thinning area is taken as a chosen ratio of the inside radius of the nozzle, and the profile of thinning is assumed to follow a linear taper away from the junction. To limit computational requirements it was assumed that the damaged model would satisfy two-ply geometric symmetry, allowing consideration of ¼ of the structure. It is clear that with a study of tees with wall thinning as described above, the information provided will serve to add to that already available on the subject.

Quantitatively, the thinning damage was assumed to extend for a limited distance (Fig. 7) along the axis of the nozzle (L_n) and of the vessel (L_v). The original thickness along the diagonal line AC is represented as T_o, and the remaining thickness after corrosion by T_R. The percentage of maximum thinning is then obtained as $(T_o - T_R)/T_o \times 100\%$. A number of values were chosen for this percentage to increase generality. For the nozzle, tapering was assumed to occur in the axial direction only. The outer limiting surface of the removed material was modeled by a cone defined by a circle at the upper position and a spatial line along the inner junction curve. For the run pipe, tapering was assumed to occur in both the axial and circumferential directions away from the inner junction line. The outer limiting surface of the removed material was modeled by a spatial surface which was defined by a circle at the distant end of the thinning area, an ellipse around the junction, and a linear tapered line along the transverse plane of symmetry.

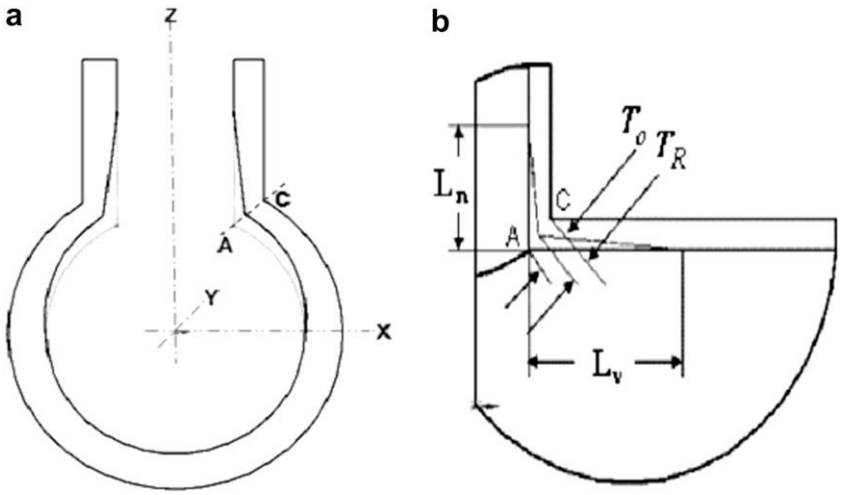

Fig. 7. Details of the assumed wall thinning: (a) full cross-sectional view in the *XZ* plane, (b) part cross-sectional view in the *YZ* plane showing enlargement of the crotch corner.

Table 5
SCF values for the preliminary wall thinning study (30% thinning).

Model	Model properties		Wall thinning extent				
	d/D	t/T	No thinning	r_i	$2r_i$[a]	Full-length tapered	Full-length uniform
PT1	0.05	0.30	2.33	2.65	2.13	3.26	2.92
PT2	0.10	0.36	2.51	2.34	2.76	3.55	2.78
PT3	0.30	0.59	3.45	3.53	5.01	5.73	3.55
PT4	0.60	0.77	4.56	6.47	6.51	6.76	7.31
PT5	0.80	0.88	6.92	8.39	8.44	8.47	11.5

[a] Extent used for the full parametric study.

A preliminary study was carried out to determine the sensitivity of the SCF on the extent of the wall thinning area. In this preliminary study, the intention was to determine the overall configuration of the wall thinning, i.e. the axial extent of thinning in each component (L_v and L_n of Fig. 7), and the circumferential extent in the vessel. As well, the difference in the results for tapered and uniform thinning was studied.

Four configurations of wall thinning were considered in the preliminary study; (1) a linear taper in thinning to a distance from the junction in the components of r_i (inner radius of nozzle), (2) a linear taper in thinning to a distance of $2r_i$, (3) a linear taper in thinning to the end of both components (90° circumferentially in the vessel), and (4) a full depth thinning to the end of both components. For each of the configurations a maximum thinning of 30% was assumed.

Results for the SCF for the four thinning configurations are given in Table 5 for five selected preliminary thinning models (PT1–PT5). These five tees are identical to models 11–15 of the full parametric study discussed below. Also given are the SCF values for the undamaged tees (0 thinning). For the models PT1 and PT2 having d/D ratios of 0.05 and 0.1 respectively, the SCF values are relatively low and the variation of the SCF is small as the extent of the wall thinning is increased. For the other three models there is a monotonic increase in the SCF. It is noted that the largest SCF values for the tapered cases occur for configuration (3), i.e. full-length tapered thinning. The SCF for models PT1–PT3 of configuration (4), i.e. full-length uniform thinning, is lower than those of the corresponding models of configuration (3). With regard to this comparison, it is to be recalled that full-length uniform thinning implies changes in the basic geometric dimensions of the models, affecting the SCF values.

For the full parametric thinning study, the geometry of configuration (2) of the preliminary study was selected (i.e. a thinning extent of $2r_i$). Fig. 8 shows the extent of the assumed thinning area for the parametric models 7–10, following this selection. With this choice, the results are expected to be generally conservative for erosion/corrosion based tapered inner-wall thinning at the junction. The values of Table 5 can be used as a means to interpolate or extrapolate for other specific extents of thinning.

8. Results for SCF without and with wall thinning

In the main wall thinning study results were determined for all 20 parametric models of Table 4, for three different conditions of geometry; (1) no thinning, (2) 20% thinning, and (3) 40% thinning. For the latter two conditions the extent of the wall thinning was according to configuration (2) as discussed in Section 7. Sample and overall results obtained for the three conditions are given in the following.

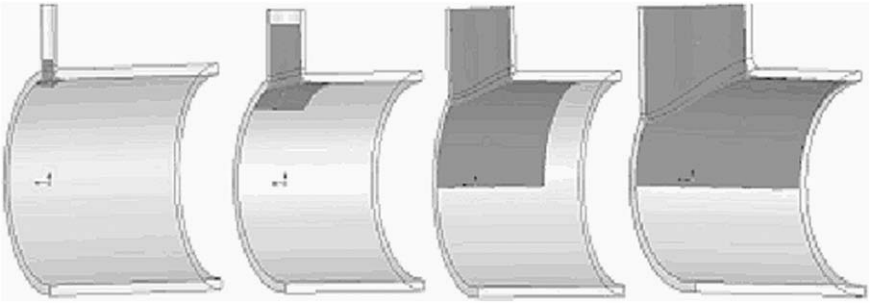

Fig. 8. (a–d) View of the assumed extent of the thinning areas (dark shading) for parametric models 7–10, showing dependence on the size of the nozzle radius.

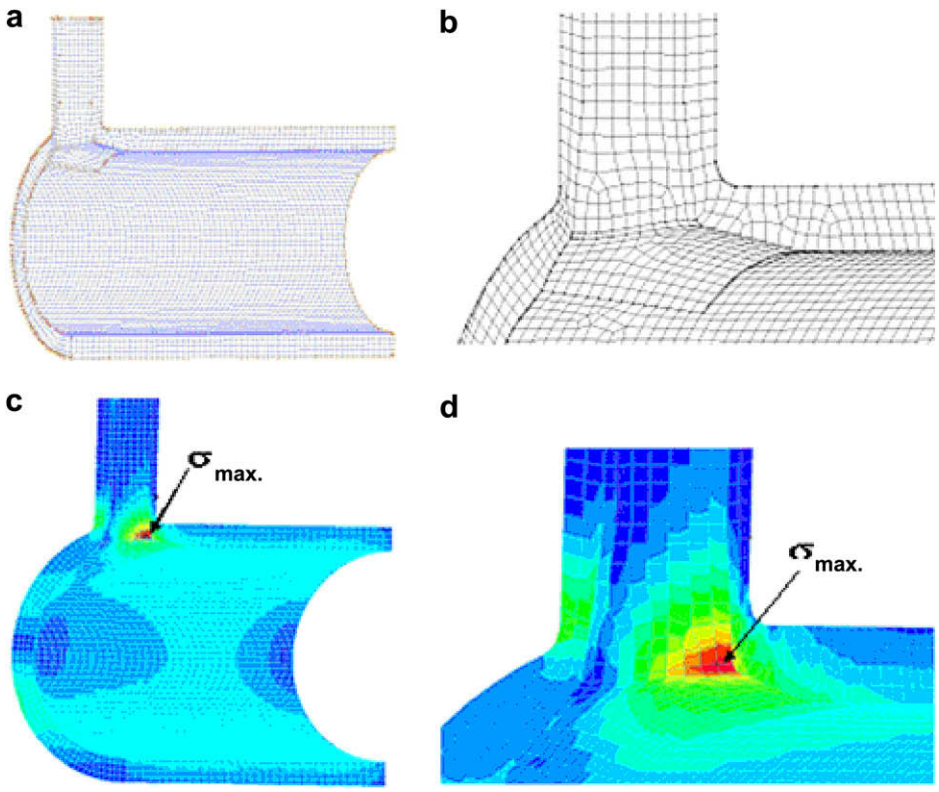

Fig. 9. Parametric model 3 with 40% thinning: (a) mesh with thinning extent, (b) magnified view of mesh near junction, (c) contour plot of von Mises stress for the entire model, (d) magnified view of contour plot near the junction.

In Fig. 9 are shown the mesh and von Mises stress contour plots on the inside surface for the parametric model 3 with 40% thinning. The enlarged view of the mesh clearly shows the thinning profile in the vessel and nozzle at the junction. The enlarged view of the contour plot clearly shows the concentration of the von Mises stress on the inside surface at the crotch corner of the tee.

Von Mises stress contours are shown in Fig. 10 for the inside and outside surfaces of the parametric model 10, with 40% thinning. It is observed that the distribution and intensity of the von Mises stress are different for the inside and outside surfaces. The highest stress is at the junction, for both the inside and outside surfaces, with the globally largest value located on the inside surface. The overall maximum stress is again at the crotch corner (position A of Fig. 1b).

Plots of the SCF against the d/D ratio are shown in Fig. 11 for each of the four main groups of the parametric models, for the three conditions; no thinning, and 20% and 40% thinning. The first two groups of the parametric models (schedules XXS and XS), which comprise of comparatively thick components, show a decrease in

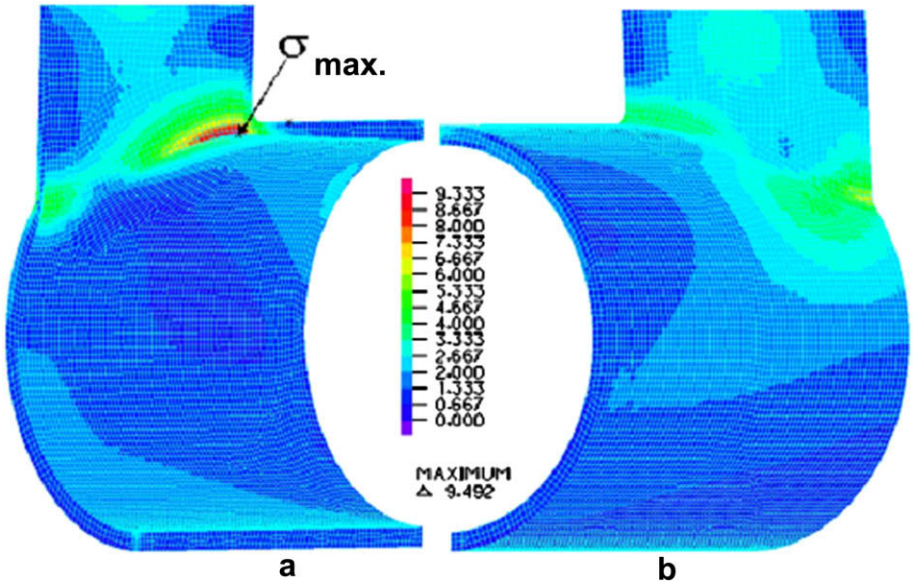

Fig. 10. Contours of von Mises stress for parametric model 10 with 40% thinning: (a) inside surface, (b) outside surface.

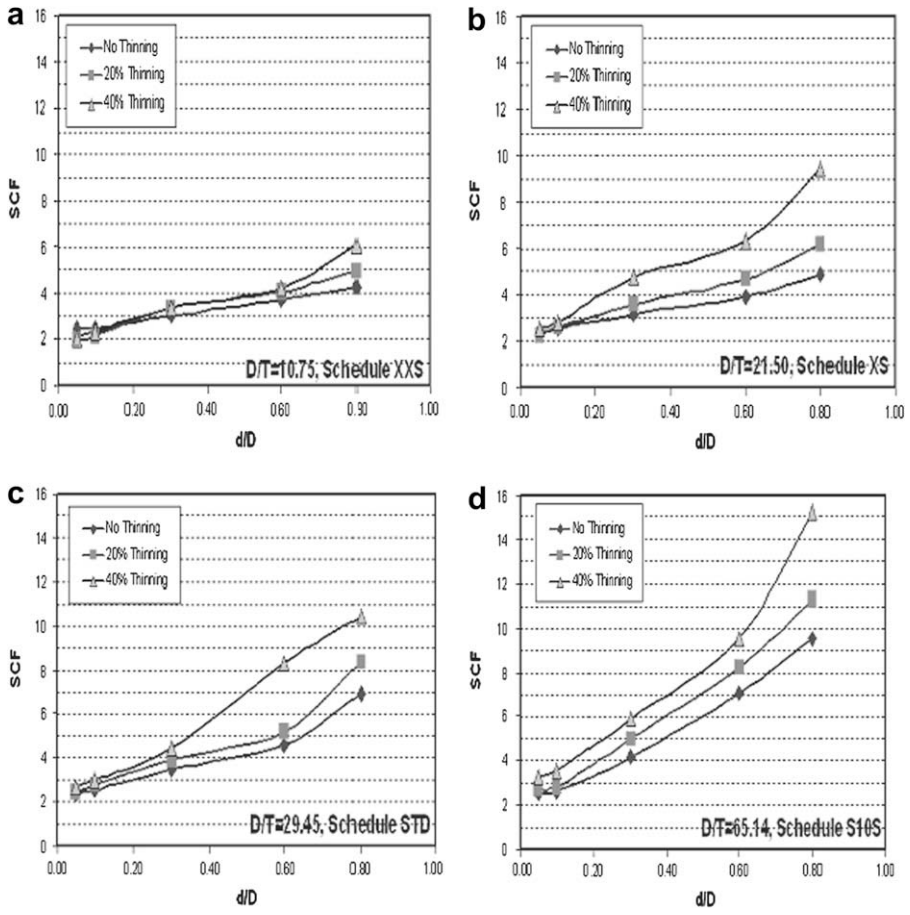

Fig. 11. (a–d) Effect on SCF of the wall thinning percentage for different pipe schedules.

the SCF when the thinning percentage is increased, at small values of the diameter ratio ($d/D < 0.2$). For larger values of the diameter ratio ($d/D > 0.2$), however, there is a modest to sizeable increase in the SCF as the thinning percentage is increased. The third and fourth groups (schedules STD and S10S) show a monotonic increase in the SCF as the thinning percentage is increased. For the fourth group a large difference in SCF values is observed (60% maximum) between the damaged and undamaged geometries. For $d/D > 0.3$, all four groups show a general increase in the rise of the SCF as the d/D ratio increases.

9. Conclusions

The current work dealing with undamaged tees serves to confirm previous SCF results, and to indicate the relative accuracy of various methods and theories. To overcome the difficulty of a mathematical singularity, and to accurately represent the weld area at the junction, a smooth transition (fillet radius) was inserted at the intersection of the outer surfaces of the two tee components. Among the significant observations was the systematic rise in the SCF value with an increase in the diameter ratio d/D, for a specified vessel diameter-thickness ratio D/T. It was also observed that for a specified d/D ratio, the SCF value increases as the D/T ratio is increased.

The current work dealing with damaged tees applies specifically to geometries with tapered inner-wall thinning having a maximum value at the junction. In general, the value of the SCF increases as the wall thinning percentage increases. For relatively thick components having small d/D ratios ($d/D < 0.2$), the effect of wall thinning is not significant. Instead, with an increase of wall thinning the SCF value may decrease, or increase very slightly. For relatively large d/D ratios ($d/D > 0.3$), the rise in the SCF with thinning percentage is more significant, and increases with the thinning percentage. For tees, without and with wall thinning damage, the largest stress is always found at the crotch corner.

Proposed future work includes determination of the fatigue characteristics of tee joints with wall thinning damage.

References

[1] Hwang KM, Woo L, Jin TE, Kim KH. A study on the shell wall thinning causes identified through experiment, numerical analysis and ultrasonic test of high-pressure feedwater heater. Nucl Eng Des 2008;238:25–32.
[2] Kim YJ, Son BG. Finite element based stress concentration factors for pipes with local wall thinning. Int J Press Vessels Piping 2004;81:897–906.
[3] Kim JW, Na MG, Park CY. Effect of local wall thinning on the collapse behavior of pipe elbows subjected to a combined internal pressure and in-plane bending load. Nucl Eng Des 2008;238:1275–85.
[4] Namita Y, Suzuki K, Abe H. Seismic proving test of eroded piping. Trans SMIRT 17, Prague, August 2003, paper K15-3, p. 1–8.
[5] Takahashi K, Kato A, Ando K, Hisasune M, Hasegawa K. Fracture and deformation behaviors of tee pipe with local wall thinning. Nucl Eng Des 2007;237:137–42.
[6] Takahashi K, Ando K, Hisasune M, Hasegawa K. Failure behavior of carbon steel pipe with local wall thinning near orifice. Nucl Eng Des 2007;237:335–41.
[7] Kim T, Moon C, Kim B. Development of the three dimensional fatigue analysis procedure for major components of the new advanced power reactor. Trans SMIRT 19, Toronto, August 2007, paper S02/3, p. 1–6.
[8] Giglio M. Fatigue analysis of different types of pressure vessel nozzle. Int J Press Vessels Piping 2003;80:1–8.
[9] Weisz E, Rauth M, Rudolph J. Fatigue behavior of oblique nozzles on cylindrical shells submitted to internal pressure and axial forces. Int J Press Vessels Piping 1998;75:473–81.

[10] Yahiaoui K, Moffat DG, Moreton DN. Cumulative damage assessment of pressurized piping branch junctions under in-plane run pipe simulated seismic bending. Int J Press Vessels Piping 1995;63:119–28.
[11] Eringen AC, Suhubi ES. Stress distribution at two normally intersecting cylindrical shells. Nucl Struct Eng 1965;2:253–70.
[12] Xue MD, Chen W, Hwang KC. Stresses at the intersection of two cylindrical shells. Nucl Eng Des 1995;154:231–8.
[13] Moini H, Mitchell TP. Stress analysis of a thick-walled pressure vessel nozzle junction. Int J Press Vessels Piping 1991;46:67–74.
[14] Dekker CJ, Stikvoort WJ. Pressure stress intensity at nozzles on cylindrical vessels: a comparison of calculation methods. Int J Press Vessels Piping 1997;74:121–8.
[15] Finlayson JP, Rothwell G, English R, Montgomery RK. Effective stress factors for reinforced butt-welded branch outlets subjected to internal pressure or external moment loads. Int J Press Vessels Piping 2003;80:311–31.
[16] Diamantoudis AT, Kermanidis T. Design by analysis versus design by formula of high strength steel pressure vessels: a comparative study. Int J Press Vessels Piping 2005;82:43–50.
[17] Lind NC. Approximate stress-concentration analysis for pressurized branch pipe connections. ASME PVP-7; 1967.
[18] Money HA. Designing flush cylinder-to-cylinder intersections to withstand pressure. ASME PVP-17; 1968.
[19] Decock J. Reinforcement method of openings in cylindrical pressure vessels subjected to internal pressure (report no. MT 104). Centre de Recherches Scientifiques et Techniques de L'Industrie des Fabrications Metalliques.
[20] Gurumurthy K, Jain R, Salpekar VY. Simplified formula for stress concentration factor in radial nozzle shell junctions under internal pressure loading. ASME PVP-430, 2001:3–6.
[21] Moffat DG, Mistry J, Moore SE. Effective stress factor correlation equations for piping branch junctions under internal pressure loading. J Press Vessel Technol 1999;121:121–6.
[22] Moffat DG, Mwenifumbo JAM, Xu SH, Mistry J. Effective stress factors for piping branch junctions due to internal pressure and external moment loads. J Strain Analysis 1991;26:84–101.
[23] Antaki GA. Pipeline and pipeline engineering – design, construction, maintenance, integrity, and repair. New York, USA: Marcel Dekker; 2003.
[24] ADINA AUI 8.2 – user interface primer and AUI command reference manual. Watertown, MA: Adina R and D Inc; 2003.
[25] ASME/ANSI B36.10/19. Carbon, alloy and stainless steel pipes.